Applied Surface Science 427 (2018) 1118–1123

Contents lists available at ScienceDirect

Applied Surface Science

journal homepage: www.elsevier.com/locate/apsusc

Full Length Article

One-step synthesis of multi-emission carbon nanodots for ratiometric temperature sensing

Vanthan Nguyen[a,b], Lihe Yan[a,*], Huanhuan Xu[a], Mengmeng Yue[a]

[a] Key Laboratory for Physical Electronicsand Devices of the Ministry of Education and Shaanxi Key Lab of Information Photonic Technique, School of Electronics and Information Engineering, Xi'an Jiaotong University, Xi'an 710049, China
[b] Le Quy Don Technical University, Hanoi 122314, Vietnam

ARTICLE INFO

Article history:
Received 24 June 2017
Received in revised form 9 August 2017
Accepted 21 August 2017
Available online 25 August 2017

Keywords:
Carbon nanodots
Multi-emission photoluminescence
Surface-related emission
Nanothermometry
Ratiometric sensors

ABSTRACT

Measuring temperature with greater precision at localized small length scales or in a nonperturbative manner is a necessity in widespread applications, such as integrated photonic devices, micro/nano electronics, biology, and medical diagnostics. To this context, use of nanoscale fluorescent temperature probes is regarded as the most promising method for temperature sensing because they are noninvasive, accurate, and enable remote micro/nanoscale imaging. Here, we propose a novel ratiometric fluorescent sensor for nanothermometry using carbon nanodots (C-dots). The C-dots were synthesized by one-step method using femtosecond laser ablation and exhibit unique multi-emission property due to emissions from abundant functional groups on its surface. The as-prepared C-dots demonstrate excellent ratiometric temperature sensing under single wavelength excitation that achieves high temperature sensitivity with a 1.48% change per °C ratiometric response over wide-ranging temperature (5–85 °C) in aqueous buffer. The ratiometric sensor shows excellent reversibility and stability, holding great promise for the accurate measurement of temperature in many practical applications.

1. Introduction

Temperature sensing is a necessity in widespread applications, such as integrated photonic devices, micro/nano electronics, biology, medical diagnostics, etc. Carrying out thermometry with greater precision, under difficult experimental circumstances, at localized small length scales or in a nonperturbative manner becomes a pressing need for the scientific community [1–3]. To this end, research into the development of fluorescent temperature sensors has attracted broad attention since they are easily miniaturized, noninvasive, accurate, and enable remote micro/nanoscale imaging [4]. Conventional fluorescent temperature sensors usually rely on intensity change of single fluorescent center, which are often susceptible to errors due to changes in probe concentration, and efficiency of excitation or detection. Compared with them, ratiometric temperature sensors can overcome these obstacles and improve measurement robustness and accuracy [5]. Recently, several ratiometric sensors, based on semiconductor quantum dots [6–8], polymer dots [2], metal-organic frameworks [9,10], luminescent dyes [11] have been designed to quantify temperature. However, these ratiometric temperature sensors often suffer from complex synthesis route, high toxicity, or low aqueous solubility, which has limited their further application.

To address these problems, carbon nanodots (C-dots) may be considered as a favorable candidate due to their unique combination properties of intense photoluminescence (PL), high photostability, high aqueous solubility, low toxicity, excellent biocompatibility, and cheap cost [12–14]. C-dots are promising substitutes for the present fluorescent nanomaterials of various applications, such as biological imaging [15,16], drug delivery [17], sensors [18,19], light-emitting devices [20–22], and lasers [23,24]. For sensing application, several ratiometric sensors have been designed for detections of pH [18,25], DNA [26], nitrogen dioxide [27], and metal ions [28–30]. Most notably, the reported C-dots do not possess intrinsic multi-emission and need further treatments with luminescent dyes or semiconductor quantum dots to construct ratiometric measurement, which may be less photostable and highly toxic. Few reports demonstrated successful synthesis of C-dots with intrinsic multi-emission for ratiometric sensing [31–33]; however, the C-dots exhibited poorly peak profile and low sensitive. Thus, the synthesis of C-dots with intrinsic multi-emission property for high-sensitive ratiometric sensing is still a major challenge.

* Corresponding author.
E-mail address: liheyan@mail.xjtu.edu.cn (L. Yan).

http://dx.doi.org/10.1016/j.apsusc.2017.08.133
0169-4332/

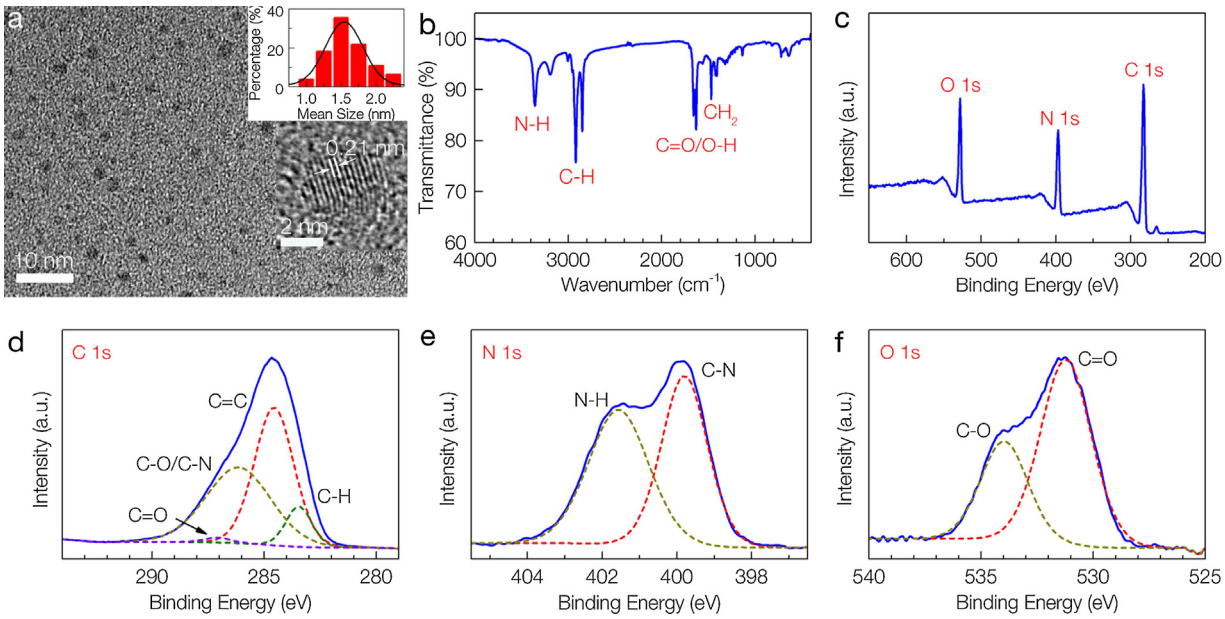

Fig. 1. Characterization of as-prepared C-dots. (a) TEM image, size distribution, and HRTEM images of the C-dots. (b) FTIR spectrum of the C-dots with the assignment of characteristic peaks. (c) XPS survey spectrum of the C-dots. (d, e, f) High-resolution XPS spectra of C 1s, N 1s, and O 1s peaks of the C-dots, respectively.

Herein, we present a simple strategy of preparing C-dots with intrinsic multi-emission property for highly sensitive ratiometric sensing of temperature. The C-dots were synthesized by one-step using femtosecond laser ablation of graphite powder in ethylenediamine. Abundant functional groups were created on the surface which form multiple surface states on the surface site and result in the multi-emission of C-dots. The as-prepared C-dots demonstrate high temperature sensitivity with a 1.48% change per °C ratiometric response over wide-ranging temperature (5–85 °C). The ratiometric sensor shows excellent reversibility and stability, holding great promise for use in many practical applications.

2. Experimental details

2.1. Preparation of C-dots

As the applications in laser processing and ultrafast optics [34–36], femtosecond lasers have been used to synthesize nanoparticles by the laser ablation in solution due to its high peak power and ultrashort pulse width [37]. In this work, C-dots were synthesized via femtosecond laser ablation of graphite powder in ethylenediamine. The details of experimental setup and procedure can be seen in our previous reports [19,38]. The laser beam (Ti: sapphire femtosecond laser system) was focused on the suspension at a laser fluence of 150 J/cm^2 by a 100 mm lens for 30 min. In our previous report, we have demonstrated that C-dots prepared with a lower raw material concentration possessed higher photoluminescence quantum yield (PLQY) [19]. In the experiment, the raw material concentration was 12.5 mg/L, and the PLQY of the C-dots solution was estimated to be 16%. After laser ablation, the suspension were centrifuged, dialyzed and the C-dots were dispersed in water for further characterization.

2.2. Characterization methods

Transmission electron microscopy (TEM) and high-resolution TEM (HRTEM) images of the C-dots were obtained via a high resolution transmission electron microscopy (model JEM–ARM200F). A UV–2600 spectrophotometer (Shimadzu) was employed to measure the absorption spectra of the samples. The Fourier transform infrared (FTIR) spectroscopy was performed on a VERTEX 70 (Bruker) using KBr pellet method. X-ray photoelectron spectroscopy (XPS) experiments were carried out on AXIS ULtrabld (Kratos) X-ray photoelectron spectrometer. The PL characterizations including emission spectra, fluorescence lifetimes, and time-resolved PL spectra were recorded using FLS920 spectrometer (Edinburgh). For the fluorescence lifetimes and time-resolved PL measurements, picosecond pulsed LED (central wavelength: 343 nm, pulse duration: <850 ps, repetition rate: 10 MHz) was used as excitation source.

2.3. Wide-field fluorescence microscopy

C-dots were immobilized on cleaned glass coverslip by dropping a small droplet of C-dots solution on coverslip. All wide-field fluorescence images were obtained via an inverted confocal microscope (Nikon C2$^+$). Laser beams (408, 488 nm) were focused on the sample via 60 × oil objective (1.49 NA) at laser intensity of ~5 mW. The fluorescence emissions was harvested at 417–477 nm, 499–529 nm, and 559–617 nm for blue, green, and red channels, respectively.

3. Results and discussion

The structure and size distribution of as-prepared C-dots were analyzed by TEM and HRTEM images. As shown in Fig. 1a, the C-dots are quasispherical and homogeneously dispersed with a narrow size distribution in the range of 1–2.5 nm. The maximum value of the fitted Gaussian peak is 1.5 nm with full width half maximum of 0.64 nm, which further confirms the narrow size distribution of as-prepared C-dots. The HRTEM image of the C-dots (inserts in Fig. 1a) show well-resolved crystal lattice fringes with a spacing of 0.21 nm which is very close to the (100) facet of graphite carbon [25]. This result indicates that the C-dots are composed of nanocrystalline core of graphitic carbon.

The chemical compositions and structures of the C-dots are investigated using FTIR and XPS analysis. The FTIR spectrum shown in Fig. 1b reveals that abundant surface functional groups are created on the surface of C-dots. For example, there are stretching vibrations of N—H bond at 3360 cm^{-1}, C—H bond at 2920 and 2850 cm^{-1}, bending vibrations of CH_2 at 1470 cm^{-1}, vibrational

absorption band of C=O/O–H bond at 1630 cm^{-1}, and the C–O bond around 1000 – 1200 cm^{-1} [39,40]. The XPS survey spectrum (Fig. 1c) shows that carbon (C 1s, 285 eV), nitrogen (N 1s, 400 eV), and oxygen (O 1s, 533 eV) elements were contained in the C-dots, and the corresponding atomic percentages are estimated to be 66.1%, 20.2%, and 13.7%, respectively. In the high-resolution spectra, C 1 s spectrum (Fig. 1d) reveal the presence of C=C (284.6 eV), C–H (283.4 eV), C–O/C–N (286.3 eV), and C=O (287.1 eV). High-resolution N 1 s spectrum (Fig. 1e) can be deconvoluted into two components, that is, C=N at 399.8 eV and N–H at 401.6 eV. The O 1 s spectrum (Fig. 1f) exhibits two peaks at 531.2 and at 540.0 eV, which are attributed to C=O and C–O groups, respectively. The results from XPS data are consistent with the FTIR analysis. The above data clearly exhibit that abundant surface functional groups are created on the surface of C-dots.

Steady-state fluorescence measurement was conducted for the C-dots dispersed in aqueous solution. Unlike many other reported C-dots [25,41], the PL emission of our sample show multiple fluorescence peaks with coexistence of both excitation-independent and excitation-dependent properties (Fig. 2). There are three obvious fluorescence peaks centered at around 400, 465, and 480 nm. The fluorescence peak at 400 nm is dominant and does not shift over an excitation ranging of 300–360 nm, while the peak at 480 nm is dominant at longer wavelength excitation of 400–460 nm. At long excitation wavelength (≥480 nm), the emission spectra shift to the red and the intensity decreases sharply as the excitation wavelength increased. Remarkably, dual emission centered at around 400 and 465 nm is present in the PL spectra when excitation ranging from 300 to 380 nm. The optimal excitation wavelength for the three PL peaks (400 nm, 465 nm, and 480 nm) are 320, 340, and 440 nm, respectively. The energy shifts of the corresponding optimal excitation wavelength are calculated to be 0.78, 0.98, and 0.24 eV. These phenomena suggest the fluorescence peaks are originated from three independent emission centers in the C-dots.

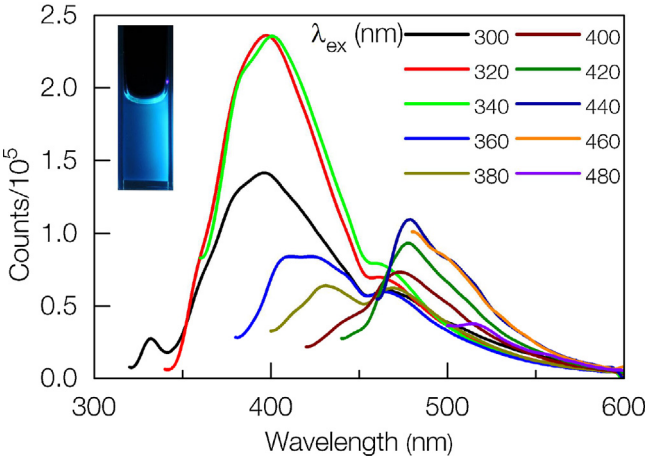

Fig. 2. The PL spectra of the C-dots. The inset is fluorescence image of C-dots solution excited with 365 nm.

The multi-emission property suggests that the as-prepared C-dots might include mutichromophoric units. Recent reports suggest that the presence of multiple chromophores could result from different surface functional groups [39,41–43]. In this mechanism, one kind of surface functional group might form a single surface state energy level and becomes an isolated emission center [39,43]. A primary question regarding C-dots fluorescence is whether the multiple emissive species are contained within a single C-dots particle or result from separate particles. In order to determine the origin of the multi-emission observed in the ensemble mea-

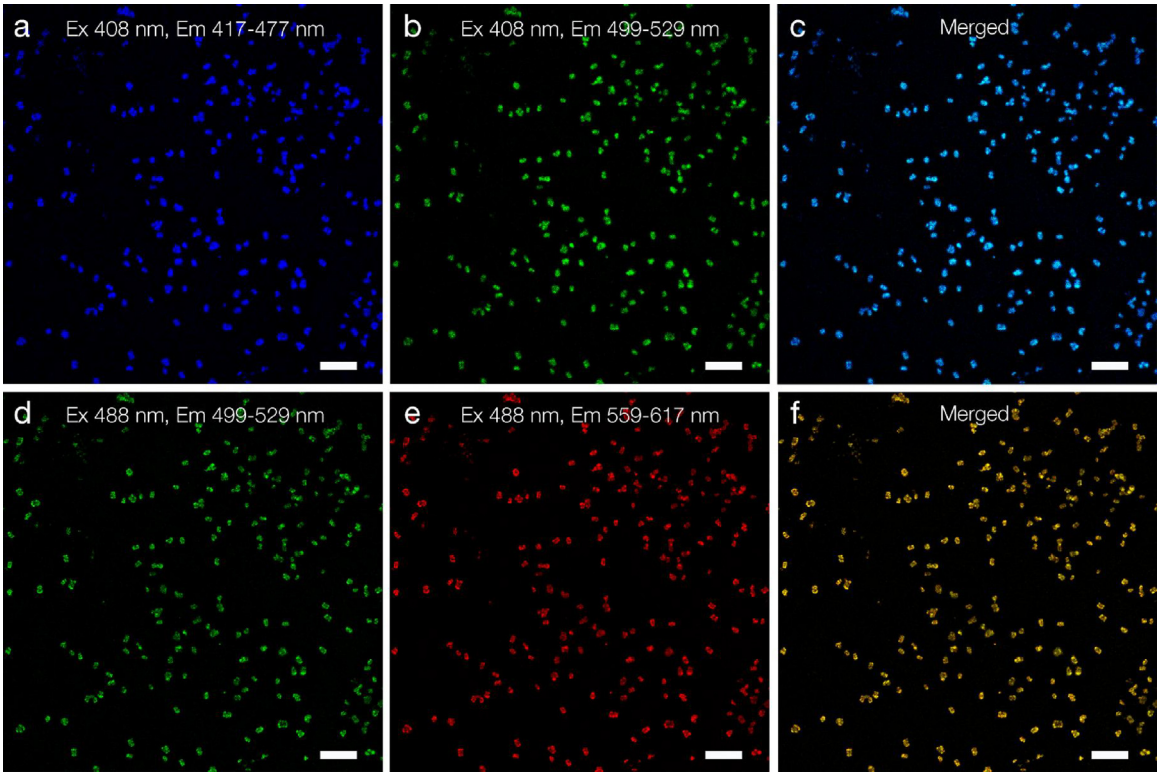

Fig. 3. Confocal microscopy fluorescence images of isolated C-dots particles. (a, b) Fluorescence images of C-dots excited at 408 nm with blue (417–477 nm) and green (499–529 nm) emissions, respectively. (c) Merged image of both blue and green emissions showing completely overlapped indicates the C-dots possess multi-color emissions. (d, e) The same field of view at 488 nm excitation with green (499–529 nm) and red (559–617 nm) emissions, respectively. (f) Merged image of both green and red emissions indicates that the C-dots possess multi-color emission (all scale bar: 2 μm). (For interpretation of the references to colour in this figure legend, the reader is referred to the web version of this article.)

surements, we performed fluorescence measurements on isolated single particles of C-dots. The C-dots were dispersed on transparent glass coverslip and wide-field fluorescence images were obtained under different excitation wavelength. Fig. 3a, b show representative fluorescence images of the C-dots particles excited at 408 nm with blue (417–477 nm) and green (499–529 nm) emissions, respectively. It should be noted that, the measured particle size using confocal microscopy is much larger than the true size of the C-dots due to the limitation of imaging resolution. Although the images are hard to reflect the size of the fluorescent particles, the locations of the fluorescent particles can be determined. From the figure, similar numbers of well-dispersed individual particles were observed in both emission channels. When Fig. 3a, b are overlaid (Fig. 3c), we observe completed overlap indicating that all of these C-dots particles can emit both blue and green fluorescence at one excitation wavelength. To determine if these C-dots particles could emit when exciting with another wavelength, the fluorescence images at the same field of view taken with 488 nm excitation were obtained. All the C-dots particles which are visible at 408 nm excitation are also apparent when excited at 488 nm in both green and red regions (559–617 nm) (Fig. 3d, e). Additionally, no new C-dots particles are visible compared with fluorescence images taken with 408 nm excitation. Similar with the aforementioned situation, completed overlap is observed when we overlaid the images of green and red emissions (Fig. 3f). The results indicate that all of these C-dots particles can absorb different wavelengths and emit multiple colors. Thus, we suggest that the multi-emission observed in the ensemble PL spectra is originated from multiple emissive species contained within a single particle rather than originating from separate particles.

In contrast to the results presented here, previous report on their fluorescence property at single-particle level indicated that C-dots particles can absorb only one wavelength and emit one specific fluorescence color [44]. This is due to the heterogeneity of C-dots particles, that is, different C-dots particles containing emissive species at different energy levels [44]. In this work, the C-dots were synthesized by laser ablation in ethylenediamine at atmosphere condition; subsequently, abundant nitrogen-, hydrogen-, oxygen-containing surface functional groups, such as C—H, C═O, C—N, N—H etc., are created on its surface. These surface functional groups might form multiple surface states on the surface site, which was confirmed by broad UV–vis absorption spectrum of C-dots (Fig. S1, Supporting Information). Furthermore, the laser ablation of graphite powder in solution can provide a short-time (on a time scale of 10^{-6}–10^{-4} s) and similar conditions of nanocluster growth and chemical reaction which result in the relatively uniform size and surface chemical structure of produced C-dots [45,46]. Thus, all of the produced C-dots particles possess multiple surface states and result in multi-emission of C-dots.

The fact that each surface state contributes to one fluorescence peak is supported by the difference in PL dynamics of different fluorescence peaks. The PL dynamics of C-dots detected at fluorescence peaks of 400 and 465 nm with 343 nm excitation are shown in Fig. 4a. Using the reconvolution fitting method, the measured time-resolved PL curves are fitted with well fit quality parameters and relaxation time scales are obtained. Both PL dynamics exhibit two distinct relaxation time scales, that is fast (1.0 ns) and slow (3.7, 5.5 ns), which can be assigned to direct excitation-recombination of carriers on the surface states and a relaxation of carriers from carbogenic-core onto the surface states, respectively [43,47]. Our previous report showed that different surface states possess different slow-decay components due to the distinct overlap degrees of photogenerated electron from carbongenic-core and hole wave functions in these surface functional groups [43]. Thus, the significant deference in the slow decays (3.7 ns and 5.5 ns for 400 and 465 nm emissions, respectively) of C-dots presented here imply

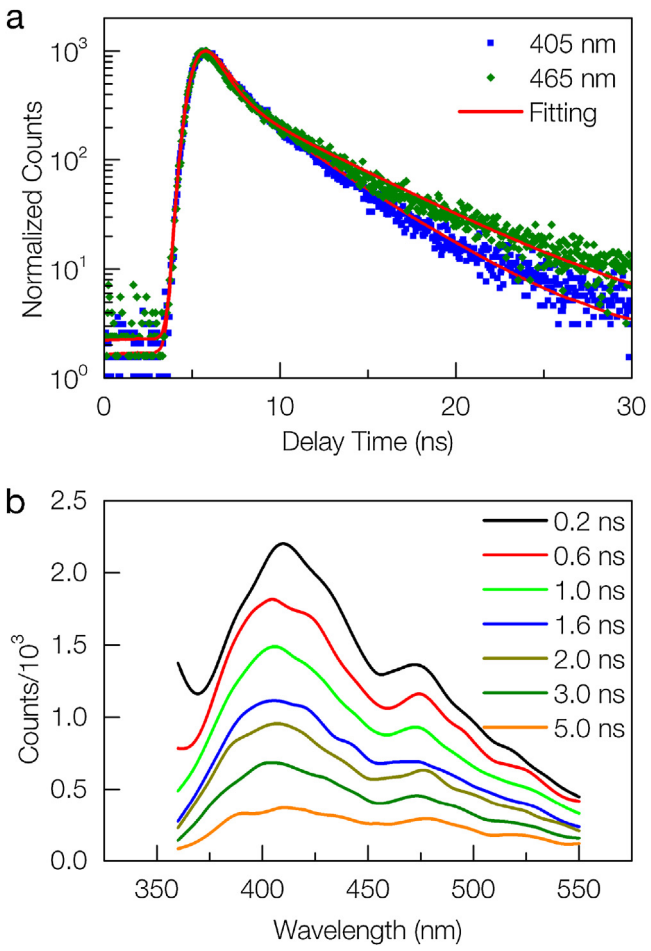

Fig. 4. (a) PL dynamics of C-dots at detected wavelengths of 400 and 465 nm with 343 nm excitation. (b) Time-resolved PL spectra of C-dots at 343 nm excitation.

that the emission centers at 400 and 465 nm are originated from two different surface states. Additionally, time-resolved PL spectra of the C-dots at 343 nm excitation exhibit two fluorescence peaks. These peaks do not shift on time scales from 0.2–5 ns (Fig. 4b) and are similar with the maximum of steady-state emission spectrum. This observation further confirms that each surface state is responsible for one fluorescence peak and these surface states are isolated without effective relaxation between the surface sites.

Finally, we investigate the temperature sensitivity of C-dots. The temperature-dependent emission spectra of the C-dots at 320 nm excitation are shown in Fig. 5a. Both fluorescence intensities of 400 and 465 nm peaks gradually decrease with the increase of temperature due to the thermal activation of nonradiative-decay pathways. The peak intensities change linearly with temperature ranging from 5 to 85 °C (Fig. 5b). Temperature-sensitive C-dots showed a fluorescence-intensities change of 3.3 and 2.1% per °C for 400 and 465 nm peaks, respectively. This indicates that the C-dots can be used as a conventional intensity-based temperature sensor with high sensitivity.

Remarkably, the unique multi-emission property makes our C-dots promise for ratiometric fluorescent temperature sensors. The ratio of the two fluorescence intensities at 400 and 465 nm (320 nm excitation) versus temperature is shown in Fig. 5c. There is a very good linear relationship between the intensity ratio and temperature in a wide temperature range from 5 to 85 °C ($R^2 = 0.998$). Thermal linearity is advantageous since it makes the correlation between peak-intensity ratio and temperature straightforward and meanwhile provides a constant thermal sensitivity along the entire

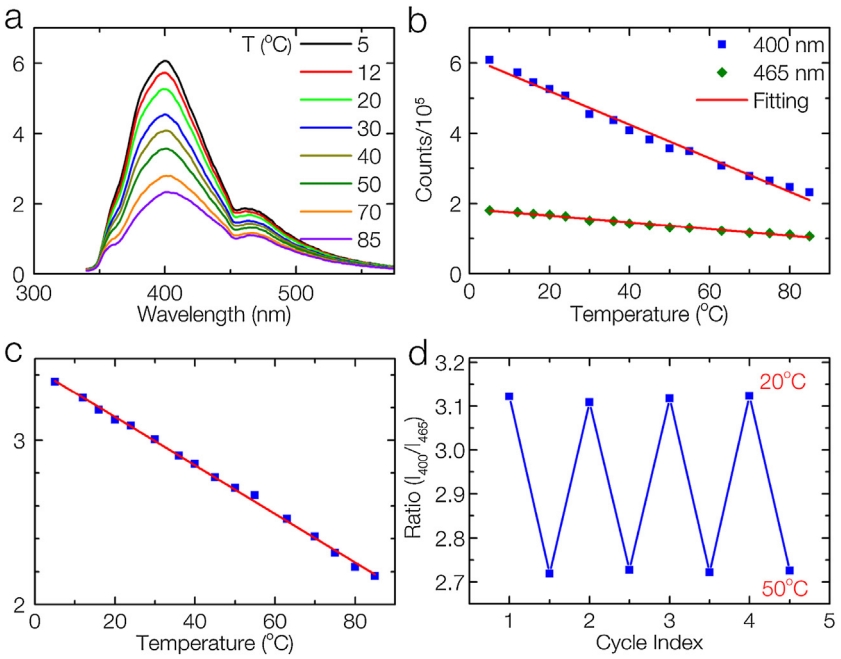

Fig. 5. (a) Emission spectra of C-dots recorded from 5 to 85 °C, excited at 320 nm. (b) Fluorescence intensities of the 400 and 465 nm peaks versus temperature. (c) The ratio of the 400 nm over the 465 nm peaks as a function of temperature. (d) Temperature reversibility study of C-dots between 20 and 50 °C.

dynamic range. The temperature-sensitivity of C-dots is determined to be 1.48% $°C^{-1}$, which is comparable with that of other materials [7–9]. It should to be noted that the temperature response range of C-dots is much wider than those of other reports on dual-emission temperature sensors and covers both the physiological temperature for biology studies and the working temperature for many electronic devices [5]. Besides 320 nm excitation, the C-dots also work at others excitation wavelengths, such as 340 and 365 nm, with high sensitivity (Fig. S2). Thus, the C-dots can be utilized for temperature sensing in many practical applications by selected different working wavelengths.

In addition, we evaluate the reversibility and stability of the ratiometric temperature sensor. The temperature-dependent emissions of C-dots were conducted between 20 and 50 °C for four cycles with 320 nm excitation (Fig. S3). The ratios of the peak intensities (I_{400}/I_{465}) at different temperatures for each cycle are almost unchanged (Fig. 5d), demonstrating the excellent reversibility of this system. Additionally, the peak intensities are evidently changed when the excitation power or sample concentration changes; however, the ratio of the peak intensities almost remain unchanged (Fig. S4). This result suggests that the C-dots sensing system is stable and robust with any changes in sample concentration, excitation, or detection efficiency.

4. Conclusions

In conclusion, C-dots with multi-emission property were synthesized by one-step method. Abundant functional groups were created on the surface which form multiple surface states on the surface site and result in the multi-emission of C-dots. The unique multi-emission property renders the C-dots as promising candidate for ratiometric temperature sensing. We demonstrate that C-dots can be utilized as an excellent ratiometric nanothermometer with a 1.48% change per °C ratiometric response over wide-ranging temperature (5–85 °C), holding great promise for use in many practical applications.

Acknowledgments

The TEM work was performed at the International Center for Dielectric Research (ICDR), Xi'an Jiaotong University, Xi'an, China. The authors also thank Mr. Ma and Ms. Lu for their help in using TEM.

This work was supported the by National Natural Science Foundation of China (Grant numbers 61235003, 11674260 and 11474078); the Natural Science Basic Research Plan in Shaanxi Province of China (Program number 2014JQ1024); and the Research Fund for the Doctoral Program of Higher Education (Grant number 20130201120025).

Appendix A. Supplementary data

Supplementary data associated with this article can be found, in the online version, at http://dx.doi.org/10.1016/j.apsusc.2017.08.133.

References

[1] Q. Li, Y. He, J. Chang, L. Wang, H. Chen, Y.W. Tan, H. Wang, Z. Shao, Surface-modified silicon nanoparticles with ultrabright photoluminescence and single-exponential decay for nanoscale fluorescence lifetime imaging of temperature, J. Am. Chem. Soc. 135 (2013) 14924–14927.
[2] F. Ye, C. Wu, Y. Jin, Y.H. Chan, X. Zhang, D.T. Chiu, Ratiometric temperature sensing with semiconducting polymer dots, J. Am. Chem. Soc. 133 (2011) 8146–8149.
[3] K. Okabe, N. Inada, C. Gota, Y. Harada, T. Funatsu, S. Uchiyama, Intracellular temperature mapping with a fluorescent polymeric thermometer and fluorescence lifetime imaging microscopy, Nat. Commun. 3 (2012) 705.
[4] X.D. Wang, O.S. Wolfbeis, R.J. Meier, Luminescent probes and sensors for temperature, Chem. Soc. Rev. 42 (2013) 7834.
[5] E.J. McLaurin, L.R. Bradshaw, D.R. Gamelin, Dual-emitting nanoscale temperature sensors, Chem. Mater. 25 (2013) 1283–1292.
[6] L. Jethi, M.M. Krause, P. Kambhampati, Toward ratiometric nanothermometry via intrinsic dual emission from semiconductor nanocrystals, J. Phys. Chem. Lett. 6 (2015) 718–721.
[7] A.E. Albers, E.M. Chan, P.M. McBride, C.M. Ajo-Franklin, B.E. Cohen, B.A. Helms, Dual-emitting quantum dot/quantum rod-based nanothermometers with enhanced response and sensitivity in live cells, J. Am. Chem. Soc. 134 (2012) 9565–9568.

[8] E.J. McLaurin, V.A. Vlaskin, D.R. Gamelin, Water-soluble dual-emitting nanocrystals for ratiometric optical thermometry, J. Am. Chem. Soc. 133 (2011) 14978–14980.
[9] Y. Cui, R. Song, J. Yu, M. Liu, Z. Wang, C. Wu, Y. Yang, Z. Wang, B. Chen, G. Qian, Dual-emitting MOF supersetdye composite for ratiometric temperature sensing, Adv. Mater. 27 (2015) 1420–1425.
[10] Y. Zhou, B. Yan, Ratiometric detection of temperature using responsive dual-emissive MOF hybrids, J. Mater. Chem. C 3 (2015) 9353–9358.
[11] X.D. Wang, X.H. Song, C.Y. He, C.J. Yang, G. Chen, X. Chen, Preparation of reversible colorimetric temperature nanosensors and their application in quantitative two-dimensional thermo-imaging, Anal. Chem. 83 (2011) 2434–2437.
[12] S.N. Baker, G.A. Baker, Luminescent carbon nanodots: emergent nanolights, Angew. Chem. Int. Ed. 49 (2010) 6726–6744.
[13] K. Hola, Y. Zhang, Y. Wang, E.P. Giannelis, R. Zboril, A.L. Rogach, Carbon dots—emerging light emitters for bioimaging, cancer therapy and optoelectronics, Nano Today 9 (2014) 590–603.
[14] F. Yuan, S. Li, Z. Fan, X. Meng, L. Fan, S. Yang, Shining carbon dots: synthesis and biomedical and optoelectronic applications, Nano Today 11 (2016) 565–586.
[15] J. Wang, F. Peng, Y. Lu, Y. Zhong, S. Wang, M. Xu, X. Ji, Y. Su, L. Liao, Y. He, Large-scale green synthesis of fluorescent carbon nanodots and their use in optics applications, Adv. Opt. Mater. 3 (2015) 103–111.
[16] S. Zhu, Q. Meng, L. Wang, J. Zhang, Y. Song, H. Jin, K. Zhang, H. Sun, H. Wang, B. Yang, Highly photoluminescent carbon dots for multicolor patterning sensors, and bioimaging, Angew. Chem. Int. Ed. 52 (2013) 3953–3957.
[17] J. Tang, B. Kong, H. Wu, M. Xu, Y. Wang, Y. Wang, D. Zhao, G. Zheng, Carbon nanodots featuring efficient FRET for real-time monitoring of drug delivery and two-photon imaging, Adv. Mater. 25 (2013) 6569–6574.
[18] W. Shi, X. Li, H. Ma, A tunable ratiometric pH sensor based on carbon nanodots for the quantitative measurement of the intracellular ph of whole cells, Angew. Chem. Int. Ed. 51 (2012) 6432–6435.
[19] V. Nguyen, L. Yan, J. Si, X. Hou, Femtosecond laser-assisted synthesis of highly photoluminescent carbon nanodots for Fe^{3+} detection with high sensitivity and selectivity, Opt. Mater. Express 6 (2016) 312–320.
[20] W. Kwon, S. Do, J. Lee, S. Hwang, J.K. Kim, S.W. Rhee, Freestanding luminescent films of nitrogen-rich carbon nanodots toward large-scale phosphor-based white-light-emitting devices, Chem. Mater. 25 (2013) 1893–1899.
[21] X. Zhang, Y. Zhang, Y. Wang, S. Kalytchuk, S.V. Kershaw, Y. Wang, P. Wang, T. Zhang, Y. Zhao, H. Zhang, T. Cui, Y. Wang, J. Zhao, W.W. Yu, A.L. Rogach, Color-switchable electroluminescence of carbon dot light-emitting diodes, ACS Nano 7 (2013) 11234–11241.
[22] W. Kwon, S. Do, J.H. Kim, M. Seok Jeong, S.W. Rhee, Control of photoluminescence of carbon nanodots via surface functionalization using para-substituted anilines, Sci. Rep. 5 (2015) 12604.
[23] W.F. Zhang, H. Zhu, S.F. Yu, H.Y. Yang, Observation of lasing emission from carbon nanodots in organic solvents, Adv. Mater. 24 (2012) 2263–2267.
[24] S. Qu, X. Liu, X. Guo, M. Chu, L. Zhang, D. Shen, Amplified spontaneous green emission and lasing emission from carbon nanoparticles, Adv. Funct. Mater. 24 (2014) 2689–2695.
[25] H. Nie, M. Li, Q. Li, S. Liang, Y. Tan, L. Sheng, W. Shi, S.X.-A. Zhang, Carbon dots with continuously tunable full-color emission and their application in ratiometric pH sensing, Chem. Mater. 26 (2014) 3104–3112.
[26] S. Huang, L. Wang, F. Zhu, W. Su, J. Sheng, C. Huang, Q. Xiao, A ratiometric nanosensor based on fluorescent carbon dots for label-free and highly selective recognition of DNA, RSC Adv. 5 (2015) 44587–44597.
[27] Y. Yan, J. Sun, K. Zhang, H. Zhu, H. Yu, M. Sun, D. Huang, S. Wang, Visualizing gaseous nitrogen dioxide by ratiometric fluorescence of carbon nanodots-quantum dots hybrid, Anal. Chem. 87 (2015) 2087–2093.
[28] A. Zhu, Q. Qu, X. Shao, B. Kong, Y. Tian, Carbon-dot-based dual-emission nanohybrid produces a ratiometric fluorescent sensor for in vivo imaging of cellular copper ions, Angew. Chem. Int. Ed. 51 (2012) 7185–7189.
[29] X. Liu, N. Zhang, T. Bing, D. Shangguan, Carbon dots based dual-emission silica nanoparticles as a ratiometric nanosensor for Cu^{2+}, Anal. Chem. 86 (2014) 2289–2296.
[30] M. Lan, J. Zhang, Y.S. Chui, P. Wang, X. Chen, C.S. Lee, H.L. Kwong, W. Zhang, Carbon nanoparticle-based ratiometric fluorescent sensor for detecting mercury ions in aqueous media and living cells, ACS Appl. Mater. Interfaces 6 (2014) 21270–21278.
[31] S. Qu, H. Chen, X. Zheng, J. Cao, X. Liu, Ratiometric fluorescent nanosensor based on water soluble carbon nanodots with multiple sensing capacities, Nanoscale 5 (2013) 5514–5518.
[32] L. Shi, X. Li, Y. Li, X. Wen, J. Li, M.M.F. Choi, C. Dong, S. Shuang, Naked oats-derived dual-emission carbon nanodots for ratiometric sensing and cellular imaging, Sens. Actuators B: Chem. 210 (2015) 533–541.
[33] F. Qu, X. Guo, D. Liu, G. Chen, J. You, Dual-emission carbon nanodots as a ratiometric nanosensor for the detection of glucose and glucose oxidase, Sens. Actuators B: Chem. 233 (2016) 320–327.
[34] J. Si, K. Hirao, Phase-matched second-harmonic generation in cross-linking polyurethane films by thermal-assisted optical poling, Appl. Phys. Lett. 91 (2007) 091105.
[35] T. Chen, J. Si, X. Hou, S. Kanehira, K. Miura, K. Hirao, Photoinduced microchannels inside silicon by femtosecond pulses, Appl. Phys. Lett. 93 (2008) 051112.
[36] Y. Ma, H. Ren, J. Si, X. Sun, H. Shi, T. Chen, F. Chen, X. Hou, An alternative approach for femtosecond laser induced black silicon in ambient air, Appl. Surf. Sci. 261 (2012) 722–726.
[37] D. Tan, S. Zhou, J. Qiu, N. Khusro, Preparation of functional nanomaterials with femtosecond laser ablation in solution, J. Photochem. Photobiol. C 17 (2013) 50–68.
[38] V. Nguyen, L. Yan, J. Si, X. Hou, Femtosecond laser-induced size reduction of carbon nanodots in solution: effect of laser fluence, spot size, and irradiation time, J. Appl. Phys. 117 (2015) 084304.
[39] L. Wang, S.J. Zhu, H.Y. Wang, S.N. Qu, Y.L. Zhang, J.H. Zhang, Q.D. Chen, H.L. Xu, W. Han, B. Yang, H.B. Sun, Common origin of green luminescence in carbon nanodots and graphene quantum dots, ACS Nano 8 (2014) 2541–2547.
[40] D. Tan, S. Zhou, B. Xu, P. Chen, Y. Shimotsuma, K. Miura, J. Qiu, Simple synthesis of ultra-small nanodiamonds with tunable size and photoluminescence, Carbon 62 (2013) 374–381.
[41] H. Ding, S.B. Yu, J.S. Wei, H.M. Xiong, Full-color light-emitting carbon dots with a surface-state-controlled luminescence mechanism, ACS Nano 10 (2016) 484–491.
[42] S. Ghosh, A.M. Chizhik, N. Karedla, M.O. Dekaliuk, I. Gregor, H. Schuhmann, M. Seibt, K. Bodensiek, I.A. Schaap, O. Schulz, A.P. Demchenko, J. Enderlein, A.I. Chizhik, Photoluminescence of carbon nanodots: dipole emission centers and electron-phonon coupling, Nano Lett. 14 (2014) 5656–5661.
[43] V. Nguyen, J. Si, L. Yan, X. Hou, Direct demonstration of photoluminescence originated from surface functional groups in carbon nanodots, Carbon 108 (2016) 268–273.
[44] S.K. Das, Y. Liu, S. Yeom, D.Y. Kim, C.I. Richards, Single-particle fluorescence intensity fluctuations of carbon nanodots, Nano Lett. 14 (2014) 620–625.
[45] P. Blandin, K.A. Maximova, M.B. Gongalsky, J.F. Sanchez-Royo, V.S. Chirvony, M. Sentis, V.Y. Timoshenko, A.V. Kabashin, Femtosecond laser fragmentation from water-dispersed microcolloids: toward fast controllable growth of ultrapure Si-based nanomaterials for biological applications, J. Mater. Chem. B 1 (2013) 2489.
[46] V. Amendola, M. Meneghetti, What controls the composition and the structure of nanomaterials generated by laser ablation in liquid solution? Phys. Chem. Chem. Phys. 15 (2013) 3027–3046.
[47] V. Nguyen, J. Si, L. Yan, X. Hou, Electron–hole recombination dynamics in carbon nanodots, Carbon 95 (2015) 659–663.